LAWRENCE
LIVERMORE
NATIONAL
LABORATORY

UCRL-JRNL-208008

Relativistically-Compressed Exploding White-Dwarf Model for Sgr A East

D. S. P. Dearborn, J. R. Wilson, G. J. Mathews

November 15, 2004

Astrophysical Journal

Relativistically-Compressed Exploding White-Dwarf Model for Sgr A East

D. S. P. Dearborn and J. R. Wilson
Lawrence Livermore National Laboratory, Livermore, CA 94550

and

G. J. Mathews
Center for Astrophysics, Department of Physics, University of Notre Dame, Notre Dame, IN 46556

ABSTRACT

Recently, a new mechanism for Type I supernovae has been proposed whereby relativistic terms enhance the self gravity of a carbon-oxygen white dwarf as it passes near a black hole. It was suggested but not confirmed that this relativistic compression can cause the central density to exceed the threshold for pycnonuclear reactions so that a thermonuclear runaway ensues. Here, we present numerical studies of such relativistically induced explosions of white dwarfs and red giant cores of various mass (particularly a typical 0.6 $M_\odot$ white dwarf) as they pass near a 3.7×10^6 black hole like Sgr A* in the Galactic center. We confirm by hydrodynamic thermonuclear burn simulations in three spatial dimensions that white dwarfs and red giant cores do indeed ignite and explode. In fact they seem to explode even farther from the black hole than earlier estimates due to increased internal temperatures from adiabatic heating as the stars are compressed. We find that the compression is sufficiently fast that red giant cores, or young ($< 10^8$ yr) white dwarfs can even be heated to thermonuclear rather than pychnonuclear ignition. We propose that such an event might explain the observed "mixed-morphology" Sgr A East supernova remnant in the Galactic center.

1. Introduction

Recently, a new mechanism for Type I supernovae has been proposed (Wilson and Mathews 2004) whereby the pycnonuclear ignition density of a white dwarf can be achieved by relativistic enhancements of the self gravity of a white dwarf which is accelerating in the background gravitational field of a black hole. White dwarfs passing a supermassive ($M > 10^6$ $M_\odot$ black hole in a dense galactic core are particularly good candidates for this paradigm. The estimated event rate (Wilson and Mathews 2004) of a few $\times 10^{-5}$ yr^{-1} for white dwarfs exploding by this mechanism in the Galactic center make the $\sim 10,000$ yr old mixed-morphology supernova remnant Sgr A East an intriguing candidate for such events. Moreover, there are some unanswered questions from our previous studies. One is whether such models will explode. Even though the density can exceed the threshold 3×10^9 g cm^{-3} for pycnonuclear reactions, the question of whether this produces a full thermonuclear burn for the entire star was not answered in our previous paper. Furthermore, the question of how such a supernova and its remnant might appear observationally has not yet been addressed.

In this paper, therefore we explore numerical models in three spatial dimensions of a white dwarf or red-giant core passing a 3.7×10^6 $M_\odot$ black hole as a possible model for Sgr A East. We follow the thermonuclear explosion of the star and model its initial expansion within the ambient medium around the giant black hole. Although we cannot conclusively say whether Sgr A East is indeed this category of supernova, we nevertheless conclude that such events do explode and their remnant appears more-or-less similar to what is presently observed in the Galactic center, and that such events should be relatively frequent over the history of the Galaxy.

2. The Model

2.1. White-Dwarf Compression

In Wilson and Mathews (2004) white-dwarf compression was analyzed in the context of an axisymmetric general relativistic treatment of the hydrodynamic and field evolution of a white dwarf in the vicinity of a black hole. For this application a quasi-Eulerian (vanishing shift vector) gauge was adopted (Wilson and Mathews 2003) with a conformally flat metric

$$ds^2 = -\alpha dt^2 + \phi^4[dr^2 + dz^2 + r^2 d\theta^2] \quad , \qquad (1)$$

where here the z coordinate is the distance along the line of centers between the black hole and the white dwarf, and r denotes the radial coordinate perpendicular to the z axis. We utilize geometrized units ($G = c = 1$) except where otherwise noted.

This metric leads (Wilson, Mathews and Marronetti 1996; Mathews, Marronetti & Wilson 1998; Mathews & Wilson 2000; Wilson 2002; Wilson and Mathews 2003) to simple Poisson-like elliptic constraint equations which can be solved to find the conformal factor and lapse function.

$$\nabla^2\phi = -2\pi\phi^5\left[DW + E\left(\Gamma W - \frac{(\Gamma-1)}{W}\right) + \frac{1}{16\pi}K_{ij}K^{ij}\right] \quad . \qquad (2)$$

$$\nabla^2(\alpha\phi) = 2\pi\alpha\phi^5 \times \left[\frac{D(3W^2-2) + E[3\Gamma(W^2+1)-5]}{W} + \frac{7}{16\pi}K_{ij}K^{ij}\right] \quad , \qquad (3)$$

where the source terms on the r.h.s. include Lorentz contracted state variables, $D = \rho W$, $E = \epsilon\rho W$, with ρ the local proper mass-energy density, ϵ the internal energy per unit mass, and W is a Lorentz-like factor, $W = \sqrt{1 + U^i U_i}$ where U^i denotes spatial components of the four velocity.

The quantity $\Gamma \equiv 1 + P/\epsilon\rho$ is an equation of state (EOS) index. In Wilson and Mathews (2004) a standard white dwarf EOS (e.g. Salpeter 1961; Hamada & Salpeter 1961) was used to specify ϵ and/or Γ as a function of density. In the three dimensional simulations described below a somewhat improved EOS is used as described in Section 4.1.

For illustration, the momentum equation in the axially symmetric coordinates of Wilson & Mathews (2004) can be written,

$$\frac{\partial S_i}{\partial t} + 6S_i\frac{\partial \ln\phi}{\partial t} + \frac{1}{\phi^6}\frac{\partial}{\partial x^j}\left(\phi^6 S_i V^j\right) + \alpha\frac{\partial P}{\partial x^i} + \sigma\alpha\left[(1+U^2)\frac{\partial \ln\alpha}{\partial x^i} - 2U^2\frac{\partial \ln\phi}{\partial x^i}\right] - \sigma\frac{U_\perp^2}{z}\delta_{iz} = 0 \quad , \qquad (4)$$

where $\sigma \equiv D + \Gamma E$, $S_i = \sigma U_i$ is the covariant coordinate momentum density, and $U^2 \equiv U_i U^i$.

The last term in Eq. (4) is a centrifugal acceleration. It accounts for the conserved angular momentum along an unspecified third coordinate perpendicular to z. Obviously, setting this term to zero produces the simple head on collision. If this term is sufficiently large, it can stabilize the stars in orbit, or it can limit motion along z to a distance of closest approach.

The term with $\sigma\alpha\partial\ln\alpha/\partial x^i$ in Eq. (4) is the the relativistic analog of the Newtonian gravitational force. The general relativistic condition of quasi-hydrostatic equilibrium for the white dwarfs can be inferred by taking the time-stationary limit of the momentum equation (4), and transforming to instantaneously comoving three-space coordinates. This gives

$$\frac{\partial P}{\partial x^i} = -\sigma\left(\frac{\partial\ln\alpha}{\partial x^i} + U^2\left[\frac{\partial\ln\alpha}{\partial x^i} - 2\frac{\partial\ln\phi}{\partial x^i}\right]\right) \quad . \quad (5)$$

Note, that in the weak-field limit, $\phi^2 \approx \alpha^{-1}$ which reduces Eq. (5) to

$$\frac{\partial P}{\partial x^i} \approx -\sigma\frac{\partial\ln\alpha}{\partial x^i}\left(1+2U^2\right) \quad , \quad (6)$$

from which it is manifestly apparent that the terms in the square brackets of Eq. (5) do not cancel. The enhanced self gravity derives from the additional U^2 dependent terms of Eqs. (5) and (6). A calculation has been done in full general relativity in axial symmetry (Wilson 2002) and shows that effect is robust in exact relativity.

For the purposes of the present application, the enhanced self gravity can be incorporated into an effective time-dependent Newtonian gravitational constant which depends upon the speed of the white dwarf as it approaches the black hole. Hence, we write:

$$G_{eff}(t) \approx G_N \times \left(1+2U^2\right) \quad , \quad (7)$$

where G_N is the usual Newtonian gravitaional constant.

3. Event rate for SGR A*

In Wilson & Mathews (2004) an event rate of a few $\times 10^{-5}$ yr^{-1} was estimated for white dwarfs to approach and explode near the near the giant black hole Sgr A* in the Galactic center. This estimate is determined by the diffusion timescale for stars to displace from BH-avoiding orbits into black-hole intercepting orbits. This diffusion time is estimated from a loss-cone model as discussed in Syer and Ulmer (1999) and Magorrian and Tremaine (1999).

In this model the two-body relaxation timescale for a spherical cluster of stars of typical mass m_* with a density $\rho(r)$ and an isotropic density dispersion $\sigma(r)$ is given by,

$$t_r = \frac{\sigma^3}{\ln\Lambda G^2\rho m_*}, \quad (8)$$

where Λ includes dimensionless factors of order unity as well as the Coulomb logarithm. Following Binney and Tremaine (1987) and Syer and Ulmer (1999) we then can write a numerical value of:

$$t_r = \frac{1.8\times10^{10}\ \mathrm{y}}{\ln(0.4\times N)}\left(\frac{\sigma}{100\ \mathrm{km\ s^{-1}}}\right)^3 \times\left(\frac{M_\odot}{m_*}\right)\left(\frac{10^4 M_\odot\ \mathrm{pc^{-3}}}{\rho}\right) \quad , \quad (9)$$

where N is the number of stars within the characteristic radius r_b and σ is the one-dimensional velocity dispersion (Seyer & Ulmer 1999) given as

$$\sigma^2 \approx \frac{GM}{(1+p)r} \quad , \quad (10)$$

where $p \sim 2$ is the logarithmic slope of the density. The white dwarf capture rate will then be given by the rate at which white dwarfs will scatter into the loss cone.

$$\lambda_{WD} \approx \int \frac{4\pi n_{wd}(r) r^2 dr}{\ln(2/\theta_{lc}) t_r} \quad , \quad (11)$$

where $n_{wd}(r)$ is the number density of white dwarfs

$$n_{wd} = f_{wd}\rho/\langle m_{wd}\rangle \quad , \quad (12)$$

where $f_{wd} \sim 0.5$ is the mass fraction in white dwarfs and $\langle m_{wd}\rangle \sim 0.6$ M$_\odot$ is the mean white-dwarf mass. The quantity $\theta_{lc} = qGM/r^2\sigma^2$ is the angular size of the "loss cone" where q is the radius at which stars are removed from the system. The density profile $\rho(r)$ divides into inner and outer regions. The black hole dominates the gravity in the inner region so that a density profile of the form $\rho \approx r^{-2}$ and a dispersion velocity, $\sigma^2 \approx GM/3r$ is expected. In the outer region on the other hand one expects flatter density and velocity-dispersion contours. Based upon the analysis of Syer & Ulmer (1999) (cf. their figure 4) we estimate $\lambda_{WD} \sim 3\times10^{-5}\ y^{-1}$ for a typical white dwarf M$_\odot$ of 0.6 M$_\odot$. However, based upon the range and

uncertainties in the parameters ρ, σ, r_b, and M_{BH} we expect a range in λ_{WD} from up to an order of magnitude above to a couple of orders of magnitude below this number. For purposes of discussion we will adopt $\sim 3 \times 10^{-5}$ as a reasonable estimate.

For a remnant moving with a typical dispersion velocity of 100 km s^{-1} for $\sim 3 \times 10^4$ y, one would expect to find such a remnant at a distance of ~ 3 pc from Sgr A*. In this regard, it is certainly of interest that indeed such a remnant (Sgr A East) exists and has been recently analyzed (Maeda et al. 2002) with the ACIS detector aboard the *Chandra X-ray Observatory.* This remnant is centered at a distance of ≈ 3 pc from Sgr A*. In fact, Sgr A* is within the remnant outer rim. The passage of the supernova shell sometime in the past may have swept gas away from the black-hole vicinity and hence, may be responsible for the present quiescent state of Sgr A*.

Also of note is the fact that its peculiar metal abundances, along with the unusual combined radio and X-ray morphologies classifies this remnant as a metal-rich "mixed-morphology" (MM) SNR. Although, the properties of Sgr A East may be explained (Maeda et al. 2002) by a low-$M_\odot$ Type II supernova, here we explore the possibility that this SNR may be the result of a black-hole induced white-dwarf explosion.

4. Ignition Calculations

4.1. The Code, Djehuty

The simulation of a white dwarf under the influence of the Sgr A* black hole requires the ability to evolve the relevant thermonuclear reactions in three spatial dimensions (3D). For this purpose we utilize the recently developed code *Djehuty.* This code is designed to model entire stars in 3D. Developed at the Lawrence Livermore National Laboratory (LLNL), it operates in a massively parallel environment, and its performance is good on models of up to 4.2×10^6 zones running on 440 CPUs.

A more detailed description of the *Djehuty* code can be found in Bazan et al. (2003), but a brief description with updates is pertinent here. The *Djehuty* mesh is formed from logically connected blocks of hexahedral cells of variable shape. The mesh encompasses an entire star, from center to photosphere, with typical sizes between 10^6 and 10^8 meshpoints. The equation of state employed in the present study utilizes an analytic approximation by Eggleton (1983) that provides continuous thermodynamic derivatives for hydrodynamic consistency. This EOS has been improved to reproduce tabulated values (Rogers, Swenson & Iglesias 1996; Rogers & Nayfonov 2002) to much better than 1% accuracy for the entire range of conditions expected in stars between 0.7 to 50.0 $M_\odot$ (over their whole evolution). Main sequence stellar models with masses as low as 0.5 $M_\odot$ have differences of only about 2% in their envelopes.

Djehuty operates in a two-temperature (2T) mode, in which the temperatures of the matter and of the radiation field are integrated in separate flux-limited diffusion equations. Included in the diffusion equation are sources and sinks that link the radiation equation to the hydrodynamic energy and momentum equations, as well as nuclear energy production, or neutrino losses. Planck and Rosseland mean opacities from the Opal library (Rogers & Iglesias 1996) at LLNL, and Alexander (1987) opacities for the lower temperatures. The conduction coefficients for electron heat flow are obtained from the Hubbard & Lampe (1969) conductive opacities tables.

The code contains an extensive set of nuclear reaction rates and reaction network including hydrogen, helium, carbon, and oxygen burning reactions leading up to the silicon peak. Nickel/iron production results from a small nuclear statistical equilibrium (NSE) network described by Timmes, Hoffman, and Woosley (2000) that begins to operate when the temperature is sufficiently high. Coulomb screening and neutrino cooling are also implemented.

At present, the hydrodynamics and treatment of the gravitational potential are purely Newtonian. The gravity is approximated by integrating a mass-radius relation and generating a spherical potential. In addition mass points can be added to simulate the gravity of nearby objects (stars or black holes). The approximation by which the relativistic compression is simulated will be discussed in the next section.

Djehuty operates with an Arbitrary Lagrange-Eulerian (ALE) hydrodynamic method, in which an explicit Lagrangian hydrodynamic step is followed by an advection step. In stable regions, or regions of large scale coherent motion where the lagrangian mesh is modestly deformed, no advection is necessary, and the code is essentially lagrangian. In regions where sheer develops, it is necessary to relax the mesh and permit material to move between cells.

To promote hydrodynamic accuracy, and time centering for other physical processes, the hydrodynamic

step is split in half. The first sub-step is a simple explicit step. This is followed by a second sub-step in which information from both the original position, and information from the half (sub) step position are used in a predictor-corrector formalism. This allows a time-centered inclusion of radiation transport and energy production with a hydrodynamics step that is second-order accurate in both time and space. In *Djehuty,* vector quantities like position and velocity are zone centered, while scalar quantities (density, temperature, etc.) are cell centered. By splitting the hydrodynamic step, the node and cell quantities have the same effective time.

The ALE scheme implemented here was tested (Pember and Anderson 2001; Anderson, Elliot & Pember 2004) based upon a number of standard hydrodynamics tests and comparing them to an Eulerian high-order Godunov scheme. The accuracy of the two schemes was found to be generally equivalent, and the ALE scheme was determined to be much improved over an earlier comparison reported by Woodward and Colella (1984).

A one dimensional (1D) stellar evolution code was also developed for use as a platform to test the physics (equation of state, nucleosynthesis, etc.) incorporated into *Djehuty,* and to provide structure information for constructing initial 3D models. *Djehuty,* reads the 1D stellar evolution models directly, and maps the physical parameters of a realistic stellar composition, density, temperature, and pressure onto a 3D spherical grid at any given stage of evolution. The radial structure of the 1D mesh is used as a guide in zoning the 3D mesh, so that steep gradients, like thin burning shells, remain resolved.

5. Initial Conditions

To start each calculation an initial distribution of density and internal energy is taken from a one-dimensional calculation of a white dwarf in hydrostatic equilibrium. We chose a frame in which the black hole is at rest and the white dwarf is in free fall from infinity towards the black hole. With this assumption we have

$$U^2 = \frac{2GM_{BH}}{d} \quad , \tag{13}$$

where M_{BH} is the mass of the black hole, d is the distance between the white dwarf and the black hole, and U^2 is the square of the spatial components of the four velocity of the white dwarf. We parameterize the orbits by the periastron distance of closest approach, d_{min}. Then the distance evolves as:

$$\frac{d}{dt}d = sign\sqrt{U^2(1 - \frac{d_{min}}{d})} \quad , \tag{14}$$

where sign is negative during in fall, and set positive after reaching d_{min}. The gravitational field in the white dwarf is then approximated with an effective gravitational constant G_{eff} of Eq. 7, while the gravitational field of the black hole continues to use the Newtonian value G_N. The initial distance, is selected to be large enough that $G_{eff} \approx G_N$ for the 1D calculation described in the next section.

6. One-dimensional modeling of compressed white dwarfs

In order to survey the physics of the compression/explosion, we first made a series of calculations in one dimension. A set of cool (old), isothermal core, CO white dwarf models ranging from 0.55 to 1.412 $M_\odot$ were generated, and their behavior examined as they entered the strong gravitational field of a massive black hole on a parabolic orbit with a periasteron distance of 8 Schwarzschild radii. Model calculations started at a position sufficiently distant from the black hole that the hydrostatic structure was effectively unperturbed. The calculation was then run until the energy production from carbon burning exceeded neutrino cooling signaling that ignition had begun. For a black hole of 3.7×10^6 $M_\odot$, comparable to that which appears to exist at the center of the Galaxy, the time for the gravitational enhancement ($2U^2$) described by Eq. 7 to increase from $< 1\%$, to over 70% is only about 40 hours. The associated compression is sufficient to ignite any white dwarf of mass $m_{wd} \geq 0.6$ $M_\odot$. The in-fall time is slow compared to the hydrodynamic adjustment time, but very fast compared to the thermal adjustment time. As a result, the compressed models are unshocked but heated by PdV work.

Figure 1 shows regions of temperature and baryon matter density density for which either neutrino cooling or screened carbon burning dominates. Also shown are the internal temperature and density profiles for white dwarfs of various mass with and without compression as labeled. This figure highlights the fact that, as the core density approaches that of a near Chandrasekhar mass (1.4 $M_\odot$) white dwarf

($\rho \sim 3 \times 10^9$ g cm^{-3}) neutrino cooling no longer keeps up with carbon burning, and ignition ensues at the center of the star.

Figure 1 also shows that low-mass white dwarfs can be ignited in a similar manner, if they they could be sufficiently compressed. However, a star that is subject to compression heating on a timescale that is short compared to the energy transport time will warm substantially. The 0.6 $M_\odot$ compressed model shown in Figure 1 actually ignites on the normal thermonuclear side of the figure where ignition is primarily temperature sensitive instead of density sensitive. This particular model started with an isothermal core temperature of 3.5×10^7 K, corresponding to an age for a normal 0.6 $M_\odot$ C/O white dwarf of about 2×10^8 years (Hansen 1999). An older (cooler) white dwarf of this same mass would ignite pycnonuclearly with a slightly greater (0.1%) additional compression.

The combination of an isothermal core, and substantial compression results in a much larger region of the core crossing the ignition line. Figure 2 shows that in the case of the 0.6 $M_\odot$ model, the material in the inner 40% of the radius is heating towards a thermonuclear runaway (i.e. $\dot{E}_{nuc} > \dot{E}_\nu$). The behavior is even more extreme if the initial model is warm (young). Such objects have a temperature maximum that is substantially off center, and will ignite near the temperature maximum with less compression.

Returning to the cool white dwarfs, the compression required to ignite a star depends on its mass and the distance from the black hole. Figure 3 shows the distance (in Schwarzschild radii) at which ignition was found to occur in the 1D models as a function of white-dwarf mass. As expected from the canonical hypothesis for the origin of Type Ia supernovae, 1.4 $M_\odot$ models ignite without any perturbation. As the mass (and central density) is reduced, the compression necessary for Coulomb screening to ignite carbon increases. Massive white dwarfs (around 1.3 $M_\odot$) need pass only within about 100 Schwarzschild radii before they are sufficiently compressed to ignite. White dwarfs between 0.7 and 1.0 must come much closer to the black hole (between 10 and 20 Schwarzschild radii) resulting in a much smaller gravitational cross section for ignition (Wilson & Mathews 2004).

Figure 3 does not apply to low mass (1 to 1000 $M_\odot$) black holes where the tidal stretching is expected to dominate. It is, however, appropriate for black holes with $m_{BH} \geq 1000\ M_\odot$ (Wilson & Mathews 2004). As

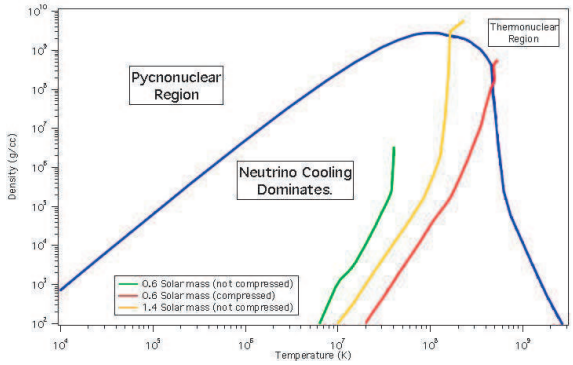

Fig. 1.— A density-temperature plot showing the regions where neutrino cooling or screened carbon burning dominates. Also shown are the temperature density structures of an uncompressed 0.6 $M_\odot$ model, a compressed 0.6 $M_\odot$, and an uncompressed 1.4 $M_\odot$ model in which the standard pycnonuclear ignition isoccurring.

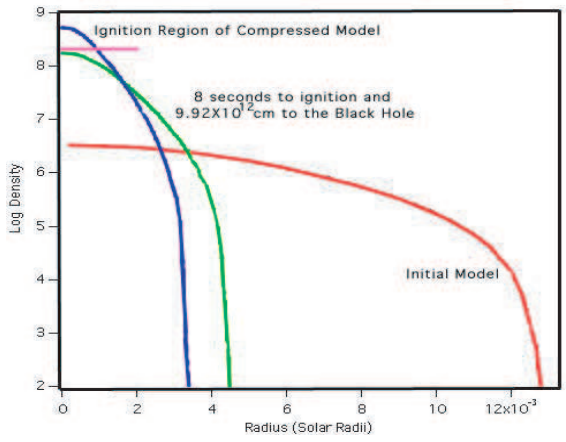

Fig. 2.— The temperature density structure of the initial 0.6 $M_\odot$ model as well as a compressed pre- and post-ignition state. The fly-by model is also shown in green.

an example of the ignition process, a 0.6 $M_\odot$ white dwarf with an internal temperature just over 3.5×10^7 K was found to ignite when the gravity had increased by 71%. At this point, the screening-enhanced carbon burning luminosity had reached 1.6×10^6 $L_\odot$, while the neutrino emission was only 1.2×10^6 $L_\odot$.

6.1. Standard 1.4 $M_\odot$ SNIa model

Since our goal is to numerically calculate a new mechanism for type I supernovae, it is instructive to first clarify the validity of the code when applied to the standard Type Ia C/O white-dwarf thermonuclear runaway. Type Ia supernovae are generally thought (cf. Thielemann et al. 2004) to occur when accretion causes the central density of a degenerate white dwarf to increase up to about 3×10^9 g cm^{-3}. At lower densities Coulomb screening can lead to carbon burning, but the heating process is limited by neutrino cooling, preventing a detonation. As the critical density is reached, the heating process is unchecked, and a thermonuclear runaway occurs.

At present, it is impossible to resolve the whole star at a scale sufficiently small (sub-centimeter) to correctly model the burn front that develops during the explosion. Hence, all simulations to date depend on a model for the burn. Without a prescription to model the burn, such as a deflagration, the expected result of carbon ignition is a detonation wave. That is what occurs in *Djehuty.* The ignition is central, resulting in a shock that propagates outward converting the entire star into iron peak elements (here ^{56}Ni). Figure 4 shows a slice through a 1.4 $M_\odot$ star just before the shock breaks through the surface. As is seen in the figure there is a small mesh-pattern asymmetry in the shock, but the result was as expected for a simulation that did not force a deflagration. Since our primary goal is not the prediction of precise abundance yields, but rather to determine whether an explosion happens. The fact that we deduce a Type Ia supernova when one is supposed to happen, and that is has about the correct explosion energy is adequate as a test for this code.

Moreover, although matching observations of the abundance yields from Type Ia requires (Thielemann et al. 2004) a deflagration model and incomplete burning of the white dwarf, we can not assume the same behavior in the externally compressed models considered here. It is generally accepted that most type 1a supernovae burn as a deflagration. This conclusion has been deduced from the observed nucleosynthe-

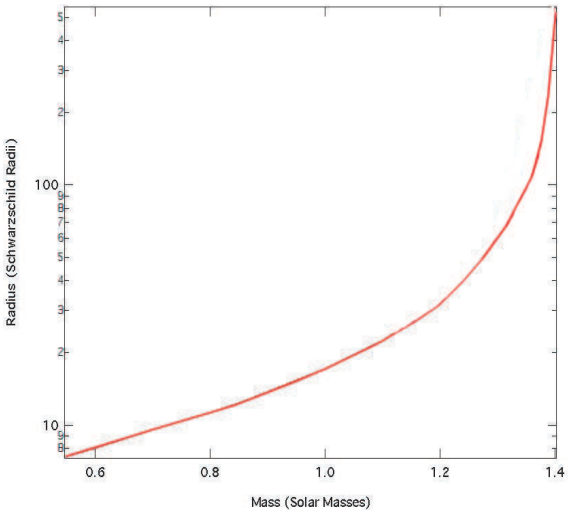

Fig. 3.— Distance from a black hole at which ignition occurs as a function of white-dwarf mass for black holes with $m_{BH} \geq 1000$ $M_\odot$. Near Chandrasekhar-mass white dwarfs are ignited at large distances from a black hole. Lower mass objects can also be ignited, but with a smaller gravitational cross section.

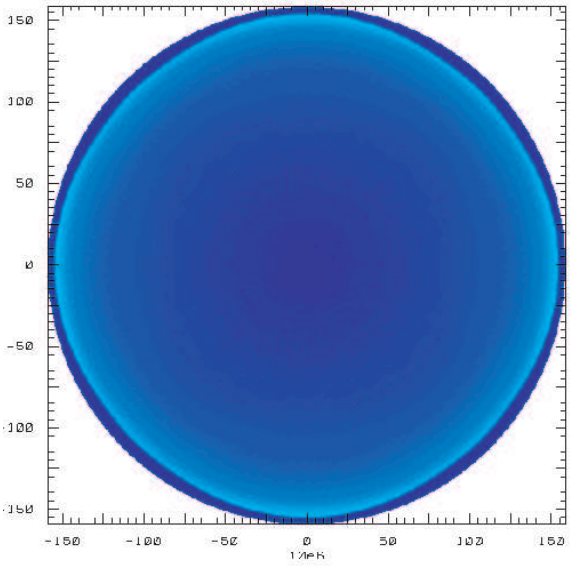

Fig. 4.— A slice through the 1.4 $M_\odot$ model shows the shock as it nears the surface.

sis yields and energetics. It is understood as arising from the rapidly growing instabilities associated with a point ignition (Bell et al. 2004). While the initial burn propagation is slow, this must evolve to a flame front traveling at a substantial fraction of the sound speed.

The situation in our models is different in a number of significant ways. In our models, there is considerable thermal heating due to the rapidity of the compression event, and the density structure is quite different from a standard 1.4 $M_\odot$ model. The white dwarf is moving at a speed of up to 1.5×10^{10} cm s^{-1} depending upon when ignition conditions are reached. This rapid approach means that the size of the region that can ignite is expanding rapidly. The compression caused by the rapid approach to the black hole thus leads to a region with many simultaneous ignition points that collide and begin to overlap each other. The increasing relativistic compression then helps maintain a density structure that resists the core expansion that characterizes a deflagration front. For these reasons, we suspect that these stars may develop a supersonic thermonuclear burn front characteristic of a detonation rather than a deflagration.

7. Three Dimensional Evolution of the Ignition models

Our initial 3D runs were started from 1D models that had just reached ignition (i.e. $\dot{E}_{nuc} > \dot{E}_\nu$). Each 1D model was mapped onto a 3D mesh located at the appropriate distance from a 3.7×10^6 $M_\odot$ black hole. It was also given a tangential velocity such that ignition would occur near periastron on a parabolic orbit. In all cases, the ignition continued in 3D and propagated to form a detonation similar to that obtained in our standard Ia 1.4 $M_\odot$ model discussed in the previous section.

As discussed in the previous section, the compression produced by this mechanism heats the isothermal core of an old white dwarf, so that a substantial region of the interior crosses the ignition line. Figure 5 shows several snapshots in the evolution of the 0.6 $M_\odot$ model after it was mapped into a 550,000 zone mesh in three dimensions. Here we see that multi-point ignition occurs over an extended region. These ignition points grow, expand, and ultimately overlap. As the burn fronts merge and move outward they become nearly spherical, and the shock arrives at the surface over a 4 ms period between 74 and 78 ms after the one-dimensional ignition and mapping to three dimensions.

As a test of resolution effects, a model with a very coarse mesh containing only 55,000 zones was run. The result was virtually identical in that there was a multi-point ignition distributed over the same core region, and the shock reached the surface about 76 ms after ignition and mapping. The nucleosynthesis yields were the same to within $\sim 2\%$.

As expected for a detonation, and shown in Table 1, the final abundance composition (for both ignition models) was nearly all (97%) Nickel. This is about the amount of Ni is necessary to produce a luminosity comparable to that of a Type Ia supernova. Kinetic energy estimates (discussed below) of the expanding star, however, suggest that only about half of the material will escape the immediate vicinity of the black hole. As discussed above, the ignition environment of a relativistically compressed star is quite different from that usually conjectured for Type Ia supernovae.

We also ran a 3D model based upon a 1.2 $M_\odot$ carbon-oxygen white dwarf that was compressed to ignition. We again used a 550,000 zones mesh, and again saw a multi-position ignition. As the ignition points merge, the velocity continues to climb, and ultimately become smoother.

The shock continues to the surface, and by 2.4 s there is considerable expansion. The small irregularities of the burn front manifest themselves as surface irregularities, but there is no evidence of the tidal distortion discussed in the next section.

The distributed ignition results in early core expansion, qualitatively like that needed to explain the nucleosynthesis seen in Type Ia supernovae. Quantitatively, however, (and at this resolution), the core expansion is not sufficient to moderate the burn front, which propagates most of the way to the surface resulting in a final composition that is substantially iron peak.

8. A 3D Pre-Ignition Fly In

In spite of the consistency of these results, we were concerned that transients that always accompany the mapping process might enhance the ignition and propagation observed. To address this possibility, we mapped a pre-ignition 0.6 $M_\odot$ model into 3D, allowing it to settle as it moved close enough to the black hole to ignite. This model was compressed in 1D to the intermediate structure (green curve) shown

TABLE 1
EJECTED ABUNDANCES (IN $M_\odot$) FOR 3D 0.6 $M_\odot$ MODELS

Nuclide	Ignition Model	Pre-Ignition Model
^{56}Ni	0.57881	0.54095
^{32}S	0.00093	0.00094
^{28}Si	0.00777	0.00720
^{24}Mg	0.00120	-
^{22}Ne	0.000001	-
^{20}Ne	0.00001	-
^{18}O	-	-
^{16}O	0.00059	0.000001
^{14}N	-	-
^{12}C	0.00008	0.00008
^{4}He	0.01062	0.04280

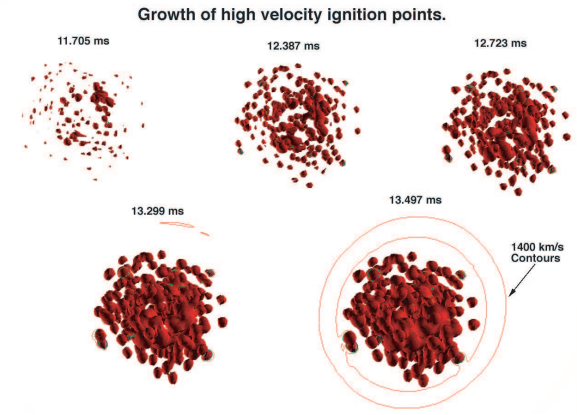

Fig. 5.— Time sequence (from 11.7 to 13.5 ms) in the development of ignition for a 0.6 $M_\odot$ model after it was mapped into a 550,000 zone mesh in three dimensions. A large number of high temperature knots ($>$ 100 keV) develop in the central region. These knots are expanding at over 2000 km s^{-1}.

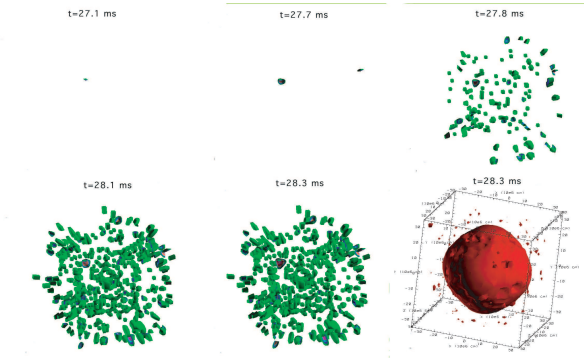

Fig. 6.— The 100 keV contours near the center of the 1.2 $M_\odot$ model are shown at 5 times. Each of these high temperature knots expands rapidly. The 300 km s^{-1} contour (red) shows a general expansion beginning in the central regions (all panels have the same scale).

in Figure 2, where the nuclear energy production rate is comparable to the neutrino loss rate, but lower. It was picked to be about 8 seconds of flight time earlier than the ignition model discussed above, so that it would have many sound crossing times permitting dynamical relaxation before ignition, as well as any tidal adjustment.

The mapping was done when the separation was 8.09 Schwarzschild radii instead of 8.04, and the gravitational enhancement factor was 1.7103 instead of 1.7156. The mapped model was given velocity components consistent with a parabolic orbit that would reach a periastron distance of 7.3 Schwarzschild radii. Figure 7 shows the parabolic orbit with the initial and ignition points indicated.

The model was evolved for 40,000 cycles or 8.4 seconds before the temperature in the ignition hot spots began the rapid climb to thermonuclear runaway. Figure 8 shows the development of the ignition and detonation at various time slices in the simulation. The model quickly leads to multipoint ignition as was seen in our earlier models. A detonation front developes, and as summarized in Table 1, the pre-ignition model burns to a final composition of 92% Ni and 7% Helium, with the remainder principally sulfur, and silicon.

There was one significant difference between these models and the models in which the mapping to 3D took place after ignition. In this pre-ignition run the ignition points were shifted to the side of the star closest to the black hole. Over the next 120 ms. the ignition points merged, and the detonation became more spherical. Nevertheless, the burned region maintained the physical shift seen in the original ignition points, and reached the surface on the leading hemisphere of the star. This aspherical behavior can be seen in the last snapshot on Figure 8.

Another difference is the time for the burn to complete. The two runs in which an already ignited 0.6 $M_\odot$ white dwarf was mapped to 3D completed their burns in about 75 ms (for both the 550,000 zone mesh and the 55,000 zone mesh). Once high temperature spots started appearing in the fly-by model, it required 120 ms for the burn to complete. This difference may be insignificant in that the 1D ignition criterion was simply that the integrated carbon burning luminosity exceeds the neutrino loss rate by a fixed amount. As *Djehuty* does not print a census of the neutrino loss rates, it is not completely clear when the 3D model crossed the ignition line as defined by the

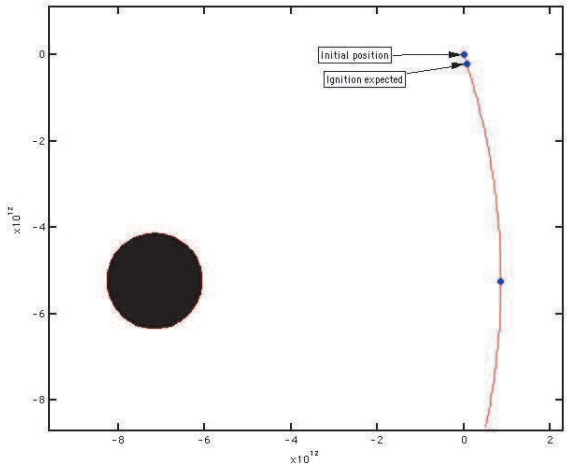

Fig. 7.— The parabolic orbit with the initial and ignition positions indicated.

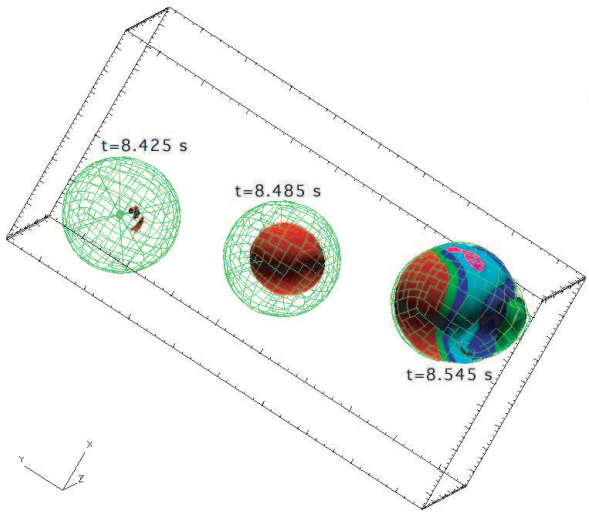

Fig. 8.— Three snapshots of the fly-by model that was mapped to 3D in a pre-ignition state, and orbited past the black hole are shown. The red regions denote contours of constant $T = 70$ keV. These regions appear within an outline of the mesh with an offset in from the center.

1D ignition runs.

While the 3D ignition occurred within a second of the expected time, the off centered distribution of ignition points suggests that though small, the tidal effect of the black hole does indeed influence this delicately balanced core structure. As described in the section on the 1D models, the ignition occurs over a substantial fraction of the radius of the star. Though the 3D model appeared quite spherical, there was a significant enhancement for ignition in the leading hemisphere.

8.1. Expansion Phase

In Figure 9 the expansion of the remnant as it passes the black hole is illustrated. The expansion phase of this run was followed for about 1500 seconds after ignition. The size of the object at 10 seconds is just visible on the scale of this figure. By 500 seconds, the size is a considerable fraction of the distance to the black hole, and tidal effects are beginning to appear. By 1500 seconds the remnant has swept past the black hole. The leading hemisphere (approximately 0.3 $M_\odot$) has positive net energy and can be expected to escape the system. Material of the trailing hemisphere has negative energy and is seen to be plunging toward orbit around the black hole.

Here again, because the burn was a detonation, the total Ni production is sufficient to power a typical Type Ia light curve. About half of that material escapes the black hole and will certainly participate in the light emission. We have not yet analyzed the residence time of the bound material to determine how long it will remain outside of the event horizon.

8.2. Temperature effect on Ignition

As discussed above, sufficient compression will lead to a density enhancement that ignites carbon burning via strong coulomb screening. However, as was shown in the 0.6 $M_\odot$ model, PdV heating can be significant, pre-igniting a model as a thermonuclear explosion instead of a pycnonuclear one. To further examine this temperature effect, we analyzed a 6 $M_\odot$ red-giant model with a hot 0.85 $M_\odot$ electron-degenerate C/O core. Removing the outer hydrogen envelope leaves behind a very hot ($> 70,000$ K) almost white dwarf with a 0.85 $M_\odot$ CO core extending 0.012 $R_\odot$ in radius. Residual helium burning occurs in an outer envelope that reaches to 0.0271 $R_\odot$. The core carbon mass fraction was 0.35 while the oxygen mass fraction was 0.63.

The core temperature structure of a very young hot white dwarf (or red giant core) is significantly different from an aged (cool) white-dwarf model. In the latter, conductive transport dominates over other energy loss mechanisms resulting in an isothermal core. In the hot model, however, the center is cooled by neutrino losses. For the model considered here, $T_c = 1.7 \times 10^8$ K. Away from the center the temperature profile is strongly peaked (up to $T = 4 \times 10^8$ K) at about 0.6 $M_\odot$ or 28% of the radius. It is the compression of this higher temperature shell that results in energy production from carbon burning. The model was subject to a 1D compression associated with passage near a 3.7×10^6 $M_\odot$ black hole. At 26.2 Schwarzschild radii, the helium burning luminosity was 1.8×10^7 $L_\odot$, and the carbon burning rate (2.0×10^6 $L_\odot$) exceeded the neutrino loss rate. We followed its approach to the black hole down to 19.6 Schwarzschild radii where the carbon burning rate (1.5×10^9 $L_\odot$) exceeded the helium burning luminosity (2×10^8 $L_\odot$).

For comparison, a cool 0.85 $M_\odot$ white dwarf with an isothermal core with $T = 2.3 \times 10^7$ K, had to penetrate in to 12.3 Schwarzschild radii to ignite. Lowering the core temperature farther to 6×10^6 K delays ignition only marginally to 12.07 Schwarzschild radii. In fact, the energy production by carbon burning was greater than the neutrino losses by the time that the star reached 12.35 Schwarzschild radii, but the temperature took longer to increase to a point where the energy production rate exceeded 10^6 $L_\odot$.

This 1D result suggests that a hot white dwarf (or the core of a red giant) can be ignited with nearly 4 times the gravitational cross section (twice the radius) of a cold white dwarf (at least when the core mass is 0.85 $M_\odot$).

The compressed red-giant-core model was also mapped to 3D and evolved with *Djehuty* to study the ignition more closely. The temperature in the carbon burning shell immediately began climbing. At about 5.5 seconds into the evolution, hot detonation spots (with $T > 100$ keV) developed in the burning shell. We have not run this model to completion, but expect that the hot spots will expand and merge as they did in the other simulations.

9. Summary/Conclusions

We have examined a proposed ignition mechanism (Wilson & Mathews 2004) in which high order gen-

eral relativistic terms lead to a compression of objects that are accelerating with respect to a strong background gravitational field. In the present work, one-dimensional initial hydrodynamic models were run to either just before or just at ignition. These models were then mapped to three dimensions to see if the ignition would sustain and detonate in the dynamical environment of a black hole passage. While the code *Djehuty* is Newtonian, its three-dimensional simulations included corrections for the general relativistic compression terms, and included the tidal stretching associated with the nearby black hole. For the massive black hole considered here, the tidal terms are estimated to be less than 10^{-7} of the compression term.

Such 3D models were run for white-dwarf masses of 0.6, 0.85, 1.2, and 1.4 $M_\odot$. All models developed into a a detonation. These detonations indeed propagate and convert substantial fractions of the star to Ni. To assure that the detonation propagation was not influenced by mapping transients, a run was preformed in which the mapping was performed many sound crossing times before ignition. The model was then flown towards the black hole and was found to detonate at the expected time.

While a sufficiently close passage can compress even a low mass cool white dwarf to ignition, it was found that the interior temperature was a significant factor in triggering the explosion. Because the orbit passage time is rapid compared to energy transport times, adiabatic heating of degenerate CO cores can lead to ignition at densities below that required for pycnonuclear ignition. Detailed modeling of the passage of what was in effect a red-giant core also led to detonation at distances even farther from the black hole. Such a detonation of a red-giant core which retained its outer hydrogen envelop would appear as a type-II supernova with a low-mass remnant shell.

In this regard, the Sgr A East remnant is certainly of interest and has been recently analyzed (Maeda et al. 2002) with the ACIS detector aboard the *Chandra X-ray Observatory*. The observed central concentration of hot X-rays which resides at $\approx 1 \pm 0.1$ arcminute from Sgr A*, corresponding to a distance of 2.3 pc for a distance of 8 kpc to the Galactic center. It has a diameter of 8.5×10 pc and an estimated age of 7500±2500 y. As noted previously, the giant black hole Sgr A* is within the outer rim of the supernova remnant, and passage of the supernova shell sometime in the past may have swept gas away from the black-hole vicinity and may be responsible for the present quiescent state of Sgr A*. Also of note is the fact that its peculiar metal abundances, along with the unusual combined radio and X-ray morphologies classifies this remnant as a metal-rich "mixed-morphology" (MM) SNR.

Although, these properties of Sgr A East may be explained (Maeda et al. 2002) by a normal low-mass Type II supernova, it may be even more consistent with the models described here. The observed ejected mass $m_{ej} < 2$ $M_\odot$ is consistent with the ejected mass $m_{ej} \sim 0.3$ $M_\odot$ for the compressed white-dwarf model (or $\sim 1-3$ $M_\odot$ for a red-giant core explosion), whereas a low-mass normal type II supernova would have ejected order 8 $M_\odot$ (Woosley &Weaver 1995).

Also, the present distance of the SNR from the central black hole in the Galactic core is consistent with this model. For a remnant to reach the observed projected distance of 2.3 pc in 7500±2500 yr would require an average projected velocity away from the black hole of $\approx 300 \pm 150$ km s^{-1}. Although this is a bit larger than the typical dispersion velocity (∼100 km s^{-1}) near the central pc of the Galaxy, it is quite typical for the observed velocity of stars which pass near to the Sgr A* black hole (Ghez et al. 1998). Moreover, the asymmetry of the explosion (cf. Figures 8 and 9) may provide some additional velocity to the escaping portion of the remnant.

Regarding the observed nucleosynthesis yields, the X-ray spectra from Sgr A* East indicate strong S, Ar, Ca, and Fe lines. The relative iron abundance in the ejecta, however is not as great ($Z_{Fe}/Z_{others} \sim 1.1$) as expected from a typical SNIa for which $Z_{Fe}/Z_{others} \sim 3$. It is, however, enhanced compared to a typical type SNII for which $Z_{Fe}/Z_{others} \sim 0.5$). This possibly implies a unique explosion of the sort not modeled here. More than one condition might have produced this explosion. Besides the 0.6 $M_\odot$ model of Table 1, a very different burn would result from a red-giant core which would ignite sooner and at higher temperature and would also have produced explosive nucleosynthesis in the outer envelopes. Another possibility which we have not modeled is that a significant fraction of white dwarfs could have Ne/O/Mg cores and masses of ~ 1.1 $M_\odot$. These would also ignite sooner than the C/O white dwarfs modeled here and probably lead to the synthesis of intermediate-mass elements as observed.

Hence, even though we have not yet established definitive nucleosynthesis yields, nor run the simula-

tions out to ages of order 10^3 to 10^4 yr corresponding to the present age of the Sgr A* East supernova remnant, we nevertheless conclude that the explosion described herein certainly could have occured and would contain many properties consistent with this supernova remnant. In a future work we will run more detailed models of the thermonuclear burn including models with red-giant cores and Ne/O/Mg white dwarfs. We will also model the evolution of the supernova remnant away from (or into) the black hole up to the present time. Such calculations will ultimately be necessary to clarify the viability of this interpretation of Sgr A* East as the result of a relativistically compressed white dwarf. Based upon the present encouraging studies such further analysis seems warranted.

Work at the Lawrence Livermore National Laboratory performed in part under the auspices of the U. S. Department of Energy under contract W-7405-ENG-48 and NSF grant PHY-9401636. Work at the University of Notre Dame supported by the US Department of Energy under Nuclear Theory grant DE-FG02-95ER40934.

REFERENCES

Alexander,D.R. & Ferguson,J.W. 1994, ApJ, 437 879

Anderson, R.W., Elliott,N.S., & Pember,R.B., 2004, J. Comp. Phys, 199, 598

Bazan, G. et al. 2003, in *3-D Stellar Evolution,* eds. Turcotte, S., Keller, S. C. & Cavallo, R. M. UCRL-PRES-144483, ASP conf. ser 293, pp. 1-15, 2003

Binney, J. & Tremaine, S. 1987, in *Galactic Dynamics*, (Princeton University Press: Princeton).

Bell, J. B., Day, M. S., Rendleman, C. A., Woosley, S. E. & Zingale, M. 2004, ApJ, 608, 883

Eggleton, P. P. (1983) MNRAS, 204, 449

Ghez, A. M., Klein, B. L., Morris, M. & Becklin, E. E. 1998, ApJ, 509, 678

Hamada, T. & Salpeter, E. E. 1961, ApJ, 134, 683

Iglasias, C. A. & Rogers, F. J. 1996, ApJ, 464, 943

Hansen, B. M. S., 1999, ApJ, 520, 680.

Hubbard,W.B. & Lampe,M. 1969, ApJS, 18, 297.

Maeda, Y. et al., 2002, ApJ, 570, 671

Magorrian, J. & Tremaine, S., 1999, MNRAS, 309, 447)

Mathews, G. J., Marronetti, P. & Wilson, J. R. 1998, PRD58, 043003

Mathews, G. J. and Wilson, J. R. 2000, Phys. Rev. D 61, 127304

Pember R. B. & Anderson R. W. 2001, in *15th American Institute of Aeronautics and Astronautics Computational Fluid Dynamics*, Anaheim, CA, Jun 11 - Jun 14, 2001, BPD 30

Salpeter, E. E. 1961, ApJ 134, 669

Syer, D. & Ulmer, A. 1999, MNRAS, 306, 35

Thielemann,F.-K., Brachwitz,F., Hflich,P., Martinez-Pinedo,G., & Nomoto,K. 2004, New Astr. Rev., 48, 605.

Timmes, F.X., Hoffman,R.A. & Woosley, S. E. 2000, ApJ, 129, 377

Wilson, J. R. 2002, PRD, 66, 084015

Wilson, J. R. & Mathews, G. J. & Marronetti, P. 1996, PRD, 54, 1317

Wilson, J. R. & Mathews, G. J., 2003, *Relativistic Numerical Hydrodynamics*, (Cambridge Univ. Press; Cambridge)

Wilson, J. R. & Mathews, G. J., 2004, ApJ, 610, 368

Woodward P. & Colella P. 1984, J Comput. Phys., 54. 115

This work was performed under the auspices of the U.S. Department of Energy by University of California, Lawrence Livermore National Laboratory under contract No. W-7405-Eng-48.

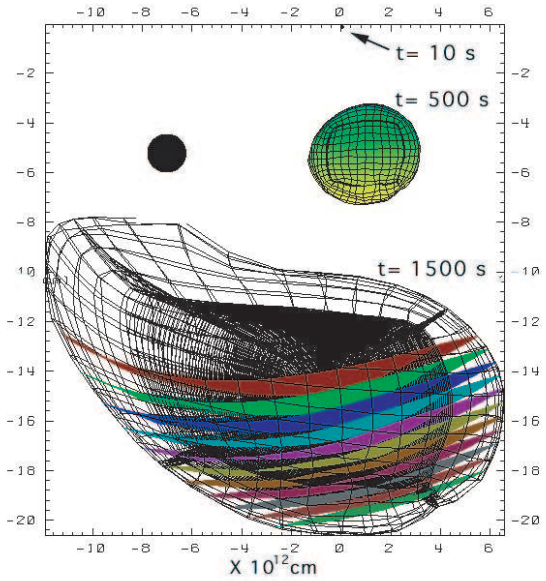

Fig. 9.— Three snapshots of the expanding supernova remnant are shown. The first two show the outer Lagrangian surface, while the last shows the mesh along with colored isopotential surfaces for regions with positive (unbound)energies.